

4-2022

MOLECULAR CLOUD PROPERTIES IN HIGH-MASS STAR FORMING REGIONS

Mohammed Essa Abdulla Ali Ahli

Follow this and additional works at: https://scholarworks.uaeu.ac.ae/all_theses

 Part of the [Physics Commons](#)



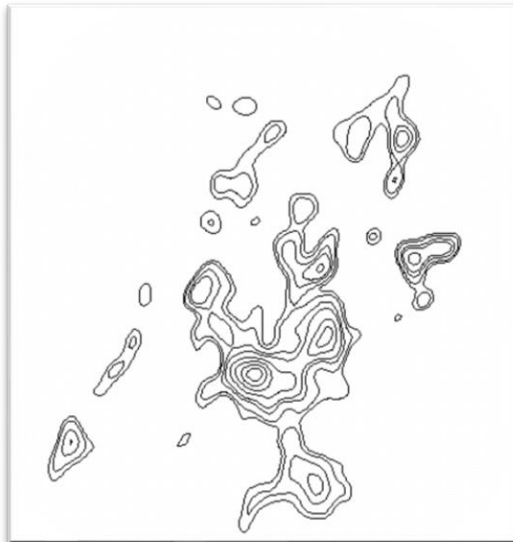
MASTER THESIS NO. 2022:6

College of Science

Department of Physics

**MOLECULAR CLOUD PROPERTIES IN HIGH-MASS
STAR FORMING REGIONS**

Mohammed Essa Abdulla Ali Ahli



April 2022

United Arab Emirates University

College of Science

Department of Physics

MOLECULAR CLOUD PROPERTIES IN HIGH-MASS
STAR FORMING REGIONS

Mohammed Essa Abdulla Ali Ahli

This thesis is submitted in partial fulfilment of the requirements for the
degree of Master of Science in Physics

April 2022

**United Arab Emirates University Master Thesis
2022:6**

Cover: $^{12}\text{CO}(2-1)$ Contours of area N42 in the Small Magellanic Cloud
(Figure: By Mohammed Ahli)

© 2022 Mohammed Essa Abdulla Ali Ahli, Al Ain, UAE

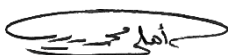
All Rights Reserved

Print: University Print Service, UAEU 2022

Declaration of Original Work

I, Mohammed Essa Abdulla Ali Ahli, the undersigned, a graduate student at the United Arab Emirates University (UAEU), and the author of this thesis entitled “*Molecular Cloud Properties in High-Mass Star Forming Regions*”, hereby, solemnly declare that this thesis is my own original research work that has been done and prepared by me under the supervision of Dr. Naslim Neelamkodan in the College of Science at UAEU. This work has not previously formed the basis for the award of any academic degree, diploma or a similar title at this or any other university. Any materials borrowed from other sources (whether published or unpublished) and relied upon or included in my thesis have been properly cited and acknowledged in accordance with appropriate academic conventions. I further declare that there is no potential conflict of interest with respect to the research, data collection, authorship, presentation and/or publication of this thesis.

Student’s Signature:



Date: 03 February 2022

Approval of the Master Thesis

This Master Thesis is approved by the following Examining Committee Members:

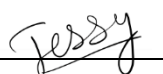
- 1) Advisor (Committee Chair): Dr. Naslim Neelamkodan
Title: Assistant professor
Department of Physics
College of Science

Signature  Date 25/04/2022

- 2) Member: Dr. Rim Fares
Title: Assistant Professor
Department of Physics
College of Science

Signature  Date 25/04/2022

- 3) Member (External Examiner): Dr. Jessy Jose
Title: Assistant Professor
Department of Physics
Institution: IISER Tirupati

Signature  Date 25/04/2022

This Master Thesis is accepted by:

Dean of the College of Science: Professor Maamar Benkraouda

Signature Maamar Benkraouda

Date May 26, 2022

Dean of the College of Graduate Studies: Professor Ali Al-Marzouqi

Signature Ali Hassan

Date May 27, 2022

Abstract

Using high spatial resolution observation of $^{12}\text{CO}(2-1)$ and $^{13}\text{CO}(2-1)$ emission, I present the molecular cloud properties of N42 in the Small Magellanic Cloud. The observations were taken using the Atacama Large Millimeter Array observations. I conducted a thorough analysis of molecular gas properties to understand how the cloud properties of N42 differ from those of Galactic clouds. My analysis shows that, in N42, the majority of CO emission appears clumpy, while molecular cores with YSOs exhibit greater linewidths and masses. Massive clump cores are associated with YSOs. Virial analysis of the ^{12}CO and ^{13}CO emissions determine the clump masses. The clumps are concluded to be in self-gravitational virial equilibrium, according to the study of velocity dispersion versus radius (σ - v) relationship. The (σ - v) relation of the ^{12}CO clumps is fitted with a power law index of 0.4 ± 0.1 . This relation in N42 has a power-law behaviour that is consistent with many Galactic clouds such as cloud N55 in the Large Magellanic Cloud irrespective of metallicity effect.

Keywords: ALMA, gravitational equilibrium, high-mass star formation, high-mass stars, HII region, molecular cloud cores, young stellar objects.

Title and Abstract (in Arabic)

خصائص السحب الجزيئية في مناطق تكوين النجوم ذات الكتلة العالية

الملخص

بإستخدام نظائر الكربون $^{12}\text{CO}(1-0)$ و $^{13}\text{CO}(1-0)$ ، أقدم خصائص السحب الجزيئية للمنطقة N42 التابعة للسحابة الماجلانية الصغيرة. تم إجراء هذا البحث بإستخدام البيانات المرصدة من مقبل مصفوفة مرصد أتاكاما المليمترى ALMA. تم إجراء تحليل شامل لخصائص الغاز الجزيئي لفهم كيفية اختلاف خصائص سحابة N42 عن خصائص السحب المجرية. تظهر غالبية انبعاثات ثاني أكسيد الكربون منكتلة في المنطقة، بينما تُظهر النوى الجزيئية التي تحتوي على أجسام نجمية فتية YSO خطوطاً وكتلاً أكبر الحجم. ترتبط الكتل ذات الحجم الكبير بالأجسام النجمية الفتية. تم احتساب كتل النوى بإستخدام نظرية القوى الكمية المطبقة على انبعاثات نظائر الكربون $^{12}\text{CO}(1-0)$ و $^{13}\text{CO}(1-0)$. وفقاً لحسابات كتل النوى تم استنتاج أن هذه النوى في حالة استقرار كمي ذاتي الجاذبية. عند رسم الكتل الجزيئية على مخطط بياني وإيجاد أفضل خط أسي للمخطط نحصل على نتيجة تفيد أن الأس 0.4 ± 0.1 وهو ما يتوافق مع العديد من السحب الجزيئية بغض النظر عن مستوى المعادن في السحابة .

مفاهيم البحث الرئيسية: تكوين النجوم، السحابة الماجلانية الصغيرة، مصفوفة مرصد أتاكاما، أجسام نجمية فتية، استقرار جاذبي.

Author Profile

Mohammed Ahli is an airline pilot by profession with over 10 years of airline flying experience for Etihad Airways. Having worked in multiple positions along his flying career he enjoyed being an aviation auditor and coding for the navigation department the most. When not flying for the airline, Mohammed flies for the UAE Air Force. Upon graduation from flight school, he went to pursue his interest in engineering and obtained his BSc in Mechanical Engineering followed by MSc in Physics. Mohammed has a wide range of interests and earned over 40 certificates in science, advances medicine, law and information technology.

Acknowledgements

My sincere thanks go to Dr. Naslim Neelamkodan, who's passion, guidance, and deep knowledge of the subject helped me throughout this journey. I'm especially grateful for all the time spent on educating and passing this knowledge on to me. Indeed, I had my own interest in the subject but with Dr. Neelamkodan's guidance I realized how much more is there to discover and learn in this field of science.

Many thanks go to the innumerable people who spent time and effort developing the software, packages, and libraries utilized throughout this research. Without them, working with astronomical data would be much more difficult.

I would like to thank all members of the Department of Science at the United Arab Emirates University for their guidance, support, and assistance throughout my studies and research.

Dedication

To all whom have nourished the seed of curiosity in me

Table of Contents

Title.....	i
Declaration of Original Work.....	iii
Approval of the Master Thesis	iv
Abstract.....	vi
Title and Abstract (in Arabic).....	vii
Author Profile.....	viii
Acknowledgements	ix
Dedication.....	x
Table of Contents	xi
List of Tables.....	xiv
List of Figures.....	xv
List of Abbreviations.....	xvi
Chapter 1: Introduction.....	1
1.1 High-mass Star Formation.....	1
1.2 Formation Mechanisms	2
1.2.1 Monolithic Collapse and Disk Accretion	2
1.2.2 Competitive Accretion.....	3
1.2.3 Proto-Stellar Collisions and Mergers.....	3
1.2.4 Wide Acceptance.....	4
1.3 Observational Support	4
1.4 High-mass Star Formation Studies with ALMA	5
1.5 GMC Scaling Relations and Clump Mass Function.....	5
1.6 Thesis Objectives.....	6
Chapter 2: Methods	8
2.1 The Data	8
2.1.1 Data Source.....	8
2.1.2 N42 Molecular Cloud.....	9
2.2 CASA	10

2.3 SAOImageDS9	13
2.4 QFitsView.....	13
2.5 Cloud Decomposition Using Astrodendro.....	15
2.5.1 Computing a Dendrogram	17
2.5.2 Exploring a Dendrogram	18
2.5.3 Saving and Loading a Dendrogram	19
2.5.4 Data Output and Visualization.....	19
2.6 Moment Maps.....	19
2.7 Clumps Mass	20
2.8 Velocity Dispersion-Size Relationship.....	21
Chapter 3: Results.....	23
3.1 Integrated Value of the Spectrum	23
3.2 Clumps Mass and Location	23
3.3 Velocity Dispersion-Size Relationship.....	26
3.4 Comparison of ^{12}CO Emission with H- α and Spitzer	28
3.5 Intensity Weighted Coordinate Map.....	30
Chapter 4: Discussion.....	32
4.1 Virial Mass Distribution	32
4.2 Histograms of ^{12}CO Emissions	32
4.3 Clump/YSO Offset	33
4.4 Velocity Dispersion-Size Relationship.....	34
4.5 H- α Map	34
Chapter 5: Conclusion	35
5.1 Molecular Cloud Properties.....	35
5.2 Distribution of Molecular Gas	35
5.3 Velocity Dispersion-Size Relationship.....	35
5.4 Intensity Weighted Coordinate Map.....	35
References	37
Appendix 1: List of Codes used	42
1.1 CASA 0th and 1st Moment Maps.....	42

1.2 Astrodendro – Generating Dendrograms.....	42
1.3 Astrodendro – Plotting Dendrograms on 0 th Moment Map.....	44
Appendix 2: N42 Astrodendro Output Table.	46

List of Tables

Table 1: List of YSO's and clumps association.....	26
--	----

List of Figures

Figure 1: A schematic of the HII region.....	1
Figure 2: An artistic view of three formation mechanism	3
Figure 3: Up, a 3x2 grid showing N42 molecular cloud	10
Figure 4: WVR calibration example.....	11
Figure 5: Phase calibration	12
Figure 6: A radio image of N42 $^{12}\text{CO}(2-1)$	13
Figure 7: Above, the original data cube.	14
Figure 8: Structure being expanded by Astrodendro's	16
Figure 9: Mapping the data back to the actual structure.....	16
Figure 10: Astrodendro graph explained	18
Figure 11: N55 clumps power law relation of 0.5	22
Figure 12: CASA output of N42 Moment 0 map	23
Figure 13: Detected clumps in the area	24
Figure 14: Plot of YSO's found in the region.....	25
Figure 15: Velocity Dispersion-Size Relationship	27
Figure 16: H- α map of N42	29
Figure 17: Spitzer 8.0 μm map of N42.....	29
Figure 18: 1 st Moment map of N42 emissions.....	31
Figure 19: Cores with YSOs and without.....	33
Figure 20: Photo-dissociation region.....	34

List of Abbreviations

ALMA	Atacama Large Millimeter/Sub-Millimeter Array
CASA	Common Astronomy Software Applications Package
EB	Execution Block
FITS	Flexible Image Transport System
GMCs	Giant Molecular Clouds
GUI	Graphic User Interface
HII	Ionized Interstellar Atomic Hydrogen
HPC	High Performance Computing
IRAC	Infrared Array Camera
ISM	Interstellar Medium
LMC	Large Magellanic Cloud
PAH	Polycyclic Aromatic Hydrocarbon
PDR	Photo-Dissociation Region
RMS	Root Mean Square
SMC	Small Magellanic Cloud
UV	Ultraviolet
WVR	Water Vapour Radiometer
YSOs	Young Stellar Objects

Chapter 1: Introduction

1.1 High-mass Star Formation

A galaxy is made up of stars, planets, and a medium of a dynamic inhomogeneous matter called the interstellar medium (ISM) that surrounds them. The matter in the ISM can take the form of a highly ionized HII (ionized interstellar atomic hydrogen) field, a neutral diffuse medium, or a molecular cloud (Figure 1), all of which can have a variety of physical and chemical properties. Ultraviolet (UV) radiation from high-mass stars, vibration, shocks, and the magnetic field all have a strong effect on these areas. The ISM is crucial to galaxy evolution because it comprises all of the matter needed to produce new stars and planets. The molecular content of the ISM in our Milky Way and surrounding galaxies has been linked to star formation, according to multi-wavelength ISM observations. H_2 is considered to be the most abundant molecule in ISM.

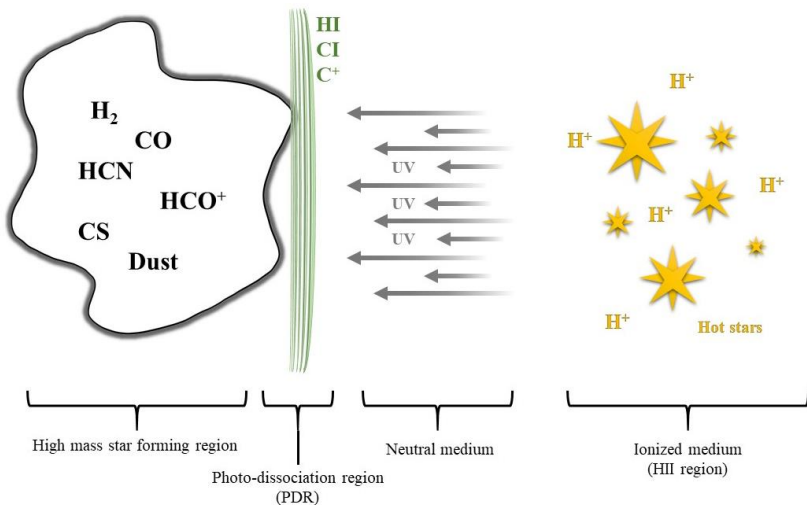


Figure 1: A schematic of the HII region around massive stars, neutral medium, PDR and GMC

Stars form in the deep interiors of giant molecular clouds (GMCs) in the ISM, which contain cold molecular gas and dust and have masses of $\sim 10^4 M_{\odot}$. The GMCs are made up of self-gravitating clumps with a number density of molecular hydrogen, $N_{H_2} > (1 - 2) \times 10^4 \text{cm}^{-3}$. The clumps collapse and form dense cores. Inside these dense molecular cores, massive stars form. (Beuther et al., 2007; Zinnecker & Yorke, 2007). GMCs are thought to be the birthplace of high-mass stars in general.

Massive stars have a major impact on the dynamics of the ISM and play an important role in galaxy evolution, but their formation mechanism is still unknown. Since they are short-lived and evolve rapidly, high-mass stars are extremely rare. The extinction of high-mass star-forming regions is extremely high, making optical observations of their early formation stages challenging. High-mass stars are often found in clusters, and their early formation process is highly complicated due to gravitational collapse, strong outflows, and ionizing radiation's effect on the local environment (Zinnecker et al., 2007; Motte, Bontemps, & Louvet, 2018). A massive proto-stellar embryo will heat and ionize the gas in its surrounding medium on its own (Spitzer, 1978). Understanding the formation of high-mass stars is thus one of the most important topics in astrophysics.

1.2 Formation Mechanisms

To describe the formation of high-mass stars, three key formation mechanisms have been suggested (Figure 2).

1.2.1 Monolithic Collapse and Disk Accretion

Self-gravitating, centrally concentrated core of gas accretes mass from fragmenting clumps in filaments (Yorke & Sonnhalter, 2002).

1.2.2 Competitive Accretion

A group of stars or a cluster of pre-stellar cores accrete mass from the gas reservoir (Bonnell et al., 1997; Bonnell, Vine, & Bate, 2004). Those with higher relative attraction will gather more material and accumulate larger masses. At a certain clump mass limit of $10M_{\odot}$, feedback in the form of radiation pressure will prevent accretion, which is a major complication with monolithic collapse and competitive accretion (Edgar & Clarke, 2003). As a result, the issue of how stars with masses greater than $10M_{\odot}$ shape arises.

1.2.3 Proto-Stellar Collisions and Mergers

In a dense cluster, proto-stars or pre-stellar cores will collide and merge to form a massive star (Bonnell, Bate, & Zinnecker, 1998). Radiation pressure feedback has no effect on the process. However, for the process to begin, a very high stellar density of massive or intermediate-mass stellar objects is needed.

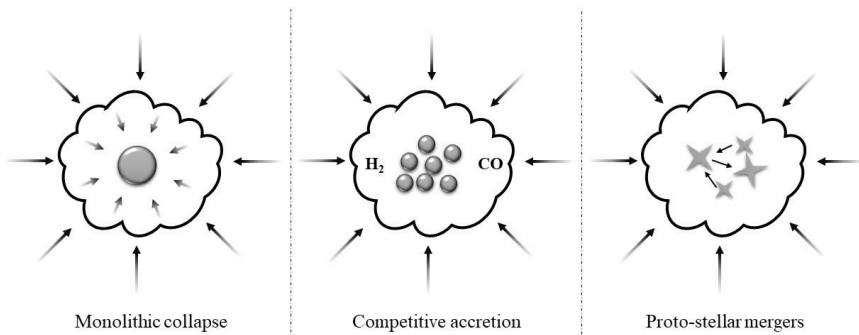


Figure 2: An artistic view of three formation mechanism of high-mass star formation

1.2.4 Wide Acceptance

The formation mechanism is determined by the molecular clouds' initial and surrounding conditions. Monolithic collapse and competitive accretion are the two scenarios of mass accretion processes that have gained widespread acceptance after years of discussion. High-mass star formation could be induced by triggering star formation at the shock compressed layers. By enhancing self-gravity due to shock compression at the cloud interface, two colliding molecular clouds (cloud-cloud collision) may lead to the formation of high-mass stars (Inoue & Fukui, 2013).

1.3 Observational Support

Given the complexity of massive star formation, a thorough comparison of theoretical predictions and empirical findings is needed to determine which accretion mechanism is significant and which physical and chemical processes are necessary. It's also crucial to see whether the cloud's initial physical properties and atmosphere have an effect on the formation process. Several pieces of evidence suggest that the atmosphere has an effect on the formation of high-mass stars. Low-mass stars are more common in stellar clusters than high-mass stars (Clarke, Bonnell, & Hillenbrand, 2000).

Another research discovered that elongated CO filament intersection areas support the cloud-cloud collision scenario since the region surveyed had large high-mass stars, while areas with low CO filaments did not. The presence of these filaments indicates a turbulent region, which is consistent with the above-mentioned forming mechanism (Fukui et al., 2015). These collisions occur at supersonic velocities of 10 to 30 km s⁻¹, implying that the cloud motion is not governed by cloud-cluster self-gravity at those speeds. The cloud-cloud collision formation method was evident in four super star clusters, but due to the small number of samples supporting

it, it is too early to conclude that cloud–cloud collision is standard (Fukui et al., 2018).

1.4 High-mass Star Formation Studies with ALMA

Atacama Large Millimeter/sub-millimeter Array (ALMA), a radio interferometric observatory, can detect molecular gas and dust emission in GMCs at scales of 0.1 pc, even in distant galaxies. The spatially resolved observations of optically thick molecules like ^{12}CO to rare isotopes like ^{13}CO and C^{18}O , as well as high-density tracers like HCN, HCO^+ , and CS in extra-galactic sources are now possible thanks to ALMA capabilities. Orion – KL, the nearest high-mass star-forming region, is one of the Milky Way's most well-studied regions, thanks to ALMA's high-spatially resolved observations. The galactic center is another fascinating extreme environment in the Milky Way, with cloud properties that are very different. ALMA observations have been used to study the high-mass star-forming regions N159, 30 Doradus, and N55 in the Large Magellanic Cloud (LMC) (Fukui et al., 2016; Indebetouw et al., 2013; Neelamkodan et al., 2018; Nayana et al., 2020). These studies found spatially resolved disks and outflows associated with newly forming massive Young Stellar Objects (YSOs) in molecular cores, as well as strong evidence of cloud accretion and cloud collision, all of which are mainstays of high-mass star formation.

1.5 GMC Scaling Relations and Clump Mass Function

A power-law relationship between velocity dispersion and clump size has been discovered in Galactic and extra-galactic clouds, suggesting self-gravitating clouds in virial equilibrium. The power law index ranges from 0.25 to 0.75. (Myers, 1983; Dame et al., 1986; Scoville et al., 1986; Solomon et al., 1987; Solomon et al., 1989; Zhou et al., 1989; Hobson, 1992; Tatematsu et al., 1998; Heyer, Carpenter, & Snell, 2001; Ikeda, Kitamura,

& Sunada, 2009). Using ^{12}CO ($J = 1 - 0$) observations, Oka et al. (2001) found significant velocity dispersions in the Galactic center clouds, indicating a divergence from a power-law relationship between velocity dispersion and radius. In the LMC, the same difference was discovered in the ^{12}CO ($J = 2 - 1$) emission of 30 Doradus cloud. External pressure is needed for cloud equilibrium confinement, according to their findings. Spatially resolved measurements of well-known molecular gas tracers (^{12}CO , HCN, HCO^+ , CS, and so on) may be used to test the velocity dispersion vs. size relationship in a variety of metallicity environments to see whether GMC characteristics follow a universal pattern.

Because of its similarity to the stellar initial mass function, the clump mass function is another essential feature of the molecular cloud population that has a direct effect on star-forming clouds. The mass distribution of the inner Milky Way clouds follows a power-law relation $\frac{dN}{dM} \propto M^{-a}$, with the index $a = 1.4-1.5$ (Kawamura et al., 1998; Yonekura et al., 1997). The cloud mass spectrum has shown the same power-law behavior in studies of local group galaxies (Wong et al., 2011). Many star-forming clouds in the Milky Way, such as Orion (Johnstone et al., 2006; Ikeda et al., 2009), the Ophiuchi cloud, and Taurus (Motte, Andre, & Neri, 1998), show this power-law behavior of the clump mass spectrum (Onishi et al., 2002). The mass spectrum index is not affected by the environments sampled, according to these reports.

1.6 Thesis Objectives

Understanding the formation of stars and molecular clouds is crucial to developing a sound theory of star formation. I want to do a thorough investigation of the metal-poor cloud N42 of the SMC. The sample area will be compared to other molecular clouds in the vicinity. ALMA was

used to collect the data for the areas. My aim is to improve our understanding of the high-mass star formation process by using multi-wavelength observations with high spatial resolution and sensitivity. This will be achieved by the following:

- 1) Study the distribution of $^{12}\text{CO}(2-1)$ and $^{13}\text{CO}(2-1)$ molecular gas emission in N42
- 2) Study how the morphology of CO molecular gas distribution is relative to the ionized gas traced by $\text{H}\alpha$ and PAH emission traced by Spitzer InfraRed Array Camera (IRAC) $8.0\ \mu\text{m}$ emission.
- 3) Study the velocity dispersion-size relationship (σ - v) in N42 compared to the molecular clouds in Milky Way and the Large Magellanic cloud. Investigate if this relationship is having any metallicity dependence.
- 4) Compare the young stellar objects (YSO) with the properties of molecular clumps to investigate the ongoing star formation in the region.

Chapter 2: Methods

2.1 The Data

2.1.1 Data Source

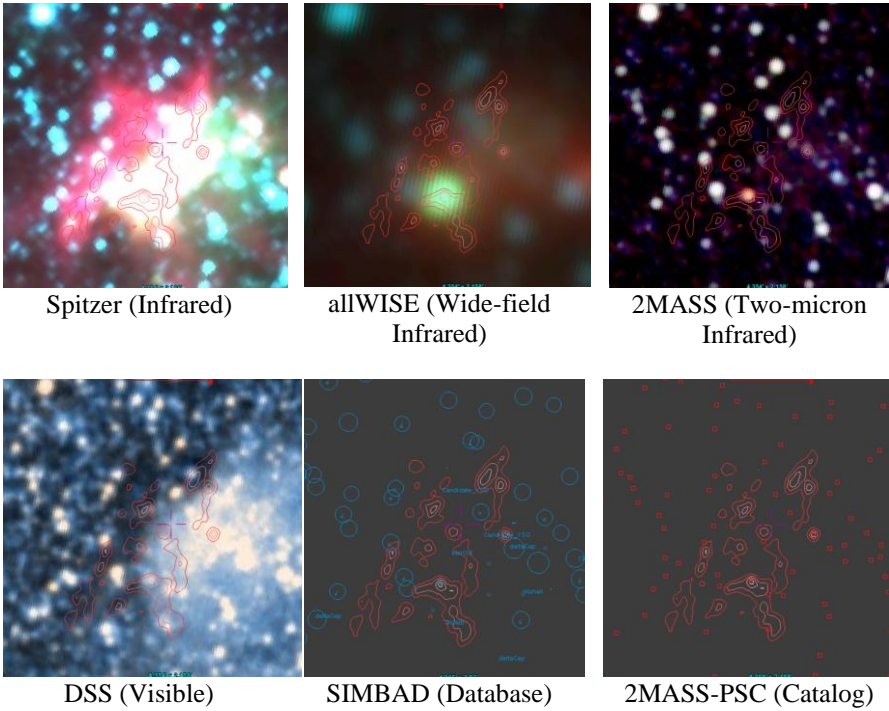
The data I am working with is obtained from Atacama Large Millimeter/submillimeter Array (ALMA), an array of separate radio telescope antennas that work together as a single telescope (interferometry) to provide higher spatial resolution images of astronomical objects. This radio array is Located in Atacama, Antofagasta, Chileon at 16,600 ft altitude. It is home for a large array of 12-meter antennae with baselines up to 16,000 meters and a total of 66 radio telescopes (Hills & Beasley, 2008). Telescope data for a selected region in space is not calibrated for many factors such as water vapor phase delay, and are not calibrated for Flux, requiring data reduction to correct, calibrate and clean up the raw data.

Working with these data can be strenuous to personal computers, thus requiring an access nod to a High-Performance Computing (HPC) to facilitate and expedite running the reduction and analysis scripts. Most of the research work will be conducted using the High-Performance Computing (HPC) facility.

The data has been retrieved from ALMA archive under the project ID: 2017-03-18T15. This project includes the observation of molecular lines $^{12}\text{CO}(2-1)$ at frequency 230 GHz and $^{13}\text{CO}(2-1)$ at 220 GHz of molecular cloud N42 of the SMC, at an spatial resolution of 0.5 arcsec and velocity resolution 320 m/s for $^{12}\text{CO}(2-1)$ data and 500 m/s for $^{13}\text{CO}(2-1)$ data.

2.1.2 N42 Molecular Cloud

N42 molecular cloud (Figure 3) lays in the northern region of the Small Magellanic Cloud (SMC). The area of study is covering a 25×25 pc square. There are fourteen YSOs in N42 that fall under three categories: reliable, possible, candidate as suggested in Sewilo et al. (2013). The locations of these YSOs will be investigated and compared to the molecular clump properties of N42 in this work. Figure 3 shows various observations of N42 for a comparison.



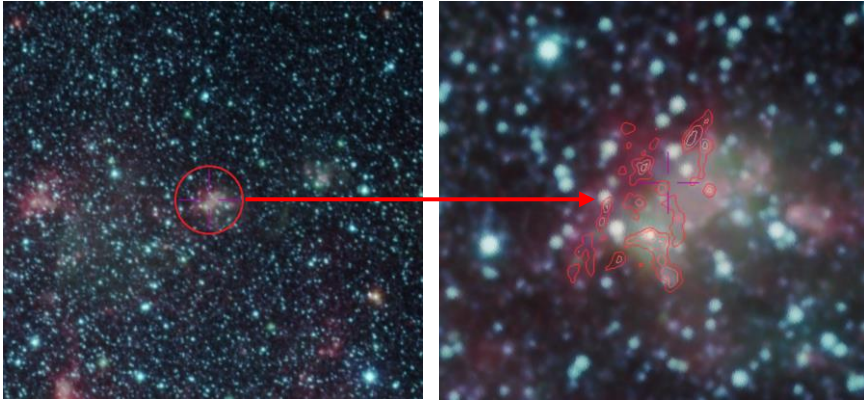


Figure 3: Up, a 3x2 grid showing N42 molecular cloud contours over different observations. Below a stacked image of all above observations for a visual reference of the study area.

The SMC is one of the Milky Way's closest galactic neighbors, a Local group galaxy, with a diameter of about 7,000 light-years at a distance of 62,000 parsec.

Even though it is a small, being classified as dwarf irregular galaxy, the SMC is so bright that it is visible to the unaided eye. Unlike the Large Magellanic Cloud (LMC; 0.5 solar metallicity), the SMC (0.2 solar metallicity) has lower metallicity; and has a gas-rich interstellar medium (ISM) (Westerlund, 1991). Studying the properties of molecular gas emission in GMCs of the SMC is therefore important for identifying, whether the metallicity of the cloud plays a role in massive star formation. The proximity to the Earth enables us to obtain high spatial resolution observation of molecular cloud cores and individual protostars.

2.2 CASA

The Common Astronomy Software Applications package (CASA) is ALMA's primary data processing software. One of the software's primary

functions is to assist in ALMA's data reduction and imaging pipelines.

An Execution Block (EB) is a basic unit of an ALMA observation. It is a self-contained sequence of measurements of the science target(s) and calibrators. Each EB consists of 60 to 90 minutes of observational data. A team of experts in data reduction at ALMA processes the observed data and performs the required calibration and imaging checks for quality assurance. Users interact with CASA using the Python language, which makes creating and running data reduction scripts a convenience (Lundgren, 2012).

Calibration due to Water Vapour Radiometer (WVR): is an early calibration step. For each EB, a WVR calibration table is produced. Each antenna's WVR detects and corrects short-timescale phase variations by measuring the rapid fluctuation of the 183 GHz water line (Figure 4).

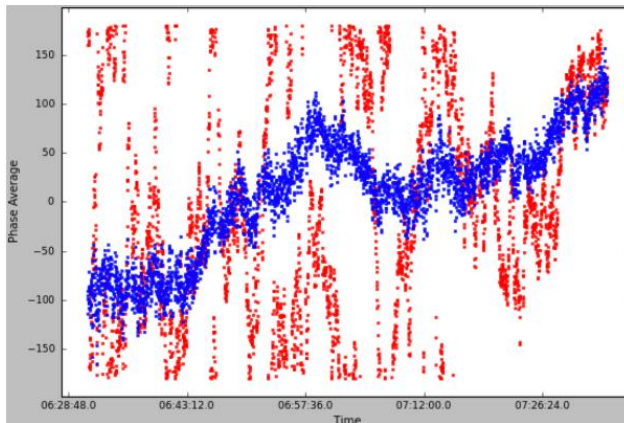


Figure 4: WVR calibration example for a 600 m baseline showing calibrated phase average in blue vs raw data in red over a period of one hour. (Credits: Perez L.)

Bandpass calibration: is the method of determining and correcting the gains that are frequency dependent. The aim is to monitor how the instrumental response changes at different frequencies. Calibrators may be used as reference points, such as bright sources with a flat and featureless spectrum.

Flux and phase calibration: flux calibration is an iterative method that determines the antenna efficiencies based on the known flux of one or more calibrators. To obtain accurate absolute flux measurements, good calibrators, such as a bright source with known shape or flux, are needed. Phase calibration, is reliant on noise level determination and image fidelity (Figure 5). The calibration for the data used in this research was performed by ALMA's calibration pipeline team using CASA.

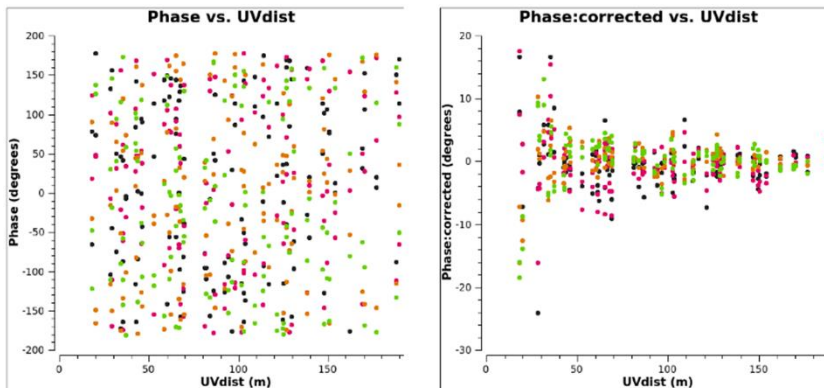


Figure 5: Phase calibration, before and after (Credits: Hoang N. T)

2.3 SAOImageDS9

SAOImageDS9, commonly known as DS9 is an astronomical imaging and data visualization standalone application with a full Graphic User Interface (GUI). DS9 supports ALMA data that are released in FITS format. DS9 supports advanced features such as 2-D, 3-D and RGB frame buffers, mosaic images, tiling, blinking, geometric markers, colormap manipulation, scaling, arbitrary zoom, cropping, rotation, pan, and a variety of coordinate systems. Using DS9 enables us to run multiple analyses and it contains various functions such as basic statistics, generating Tri-color images, and generating 2D and 3D images (Figure 6).

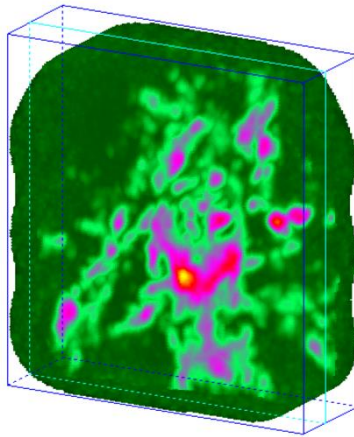


Figure 6: A radio image of N42 $^{12}\text{CO}(2-1)$ viewed in DS9 using Data Cubes 3D visualization

2.4 QFitsView

QFitsView is a full GUI software that combines features from both CASA and DS9 making it a useful tool for cross examining the previous two tools integrity. Other than validating the results from CASA and DS9, QFitsView will be used to perform quick data reduction tasks and noise

cleaning up due to its fast execution algorithms (Figure 7). This process not only removes the noise and blank areas in the data cube but also optimizes the data's size making it more efficient and faster to conduct the study while minimizing the computing power required for running the analysis. The output file after cleaning up the data cube was reduced in size by 93%.

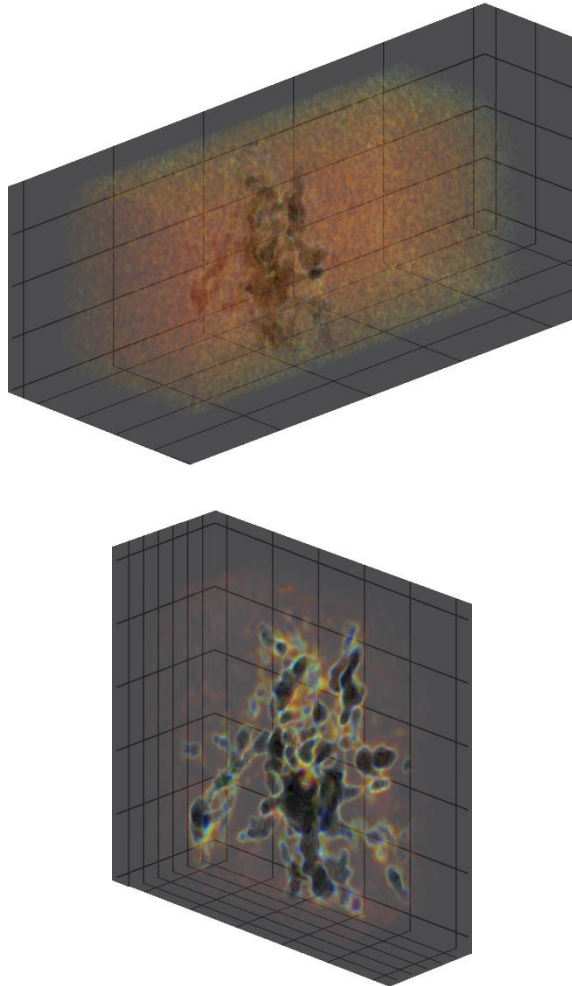


Figure 7: Above, the original data cube vs the cleaned data cube below.

2.5 Cloud Decomposition Using Astrodendro

After calibrating and refining ALMA data with CASA/QFitsView and processing it with DS9 to determine the noise value and exact data cube information we obtain the following:

```
Beam major: 2.6838 arc seconds
Beam minor: 1.8953 arc seconds
RMS: 0.19 Jy/beam
Velocity Scale: 0.32 km/s
Spatial Scale: 0.5 arc seconds
```

It is possible now to proceed and work with Astrodendro, a Python package that provides an easy method to compute dendrograms of astronomical data compatible with FITS files that we work with. This will allow us to examine the cloud properties such as velocity-dispersion, mass, and radius of the cores.

We can think of our astronomical data as the main structure (Figure 8) in which Astrodendro will represent the data in a hierarchy resembling a tree that has branches and leaves (Figure 9). Allowing us to collapse back our mapped structure with valuable details while retaining the new structured hierarchy overlay. Simply, Astrodendro will generate a dendrogram starting with a trunk (or multiple trunks) having branches and leaves where each identified structure is an iso-surface. The brightest and smallest group of pixels in the data are labeled as leaves representing what we will be referring to as cores. Clumps on the other hands are the trunks of the dendrogram; which is a formation of multiple structures that have a lower density medium.

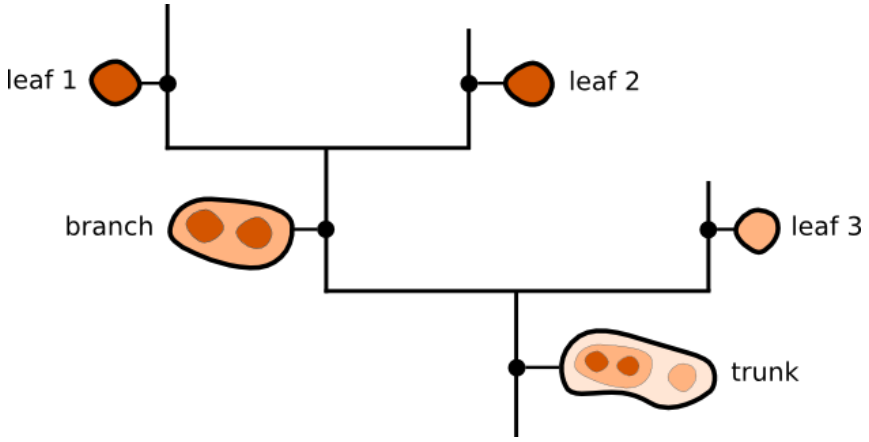


Figure 8: Structure being expanded by Astrodendro's algorithm (Credits: Astrodendro)

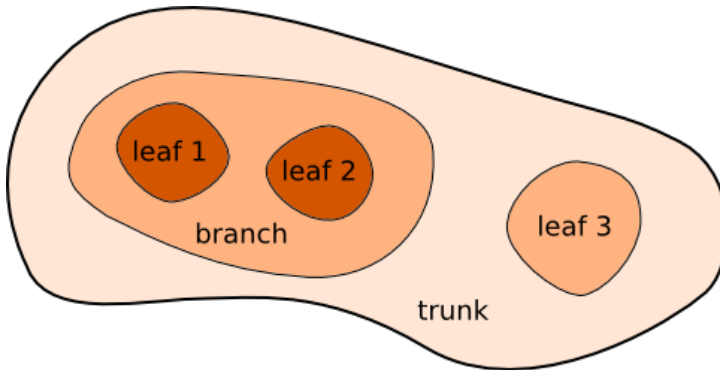


Figure 9: Mapping the data back to the actual structure without disrupting the actual data (Credits: Astrodendro)

2.5.1 Computing a Dendrogram

To compute dendrograms we use the following code in Python:

```
metadata['data_unit']=u.Jy/u.beam
metadata['spatial_scale'] = 0.5*u.arcsec
metadata['beam_major'] = 2.6838*u.arcsec
metadata['beam_minor'] = 1.8953*u.arcsec
metadata['velocity_scale'] = 0.32*u.km/u.s

data, header = fits.getdata('n42.fits',
header=True)
wcs = wcs.WCS(header)
rms=0.19 #Jy/beam
d = Dendrogram.compute(data, min_value=2*rms,
min_delta=2*rms, min_npix=1 ,verbose=True)
```

In the above code we import the Astrodendro package, followed by importing our data cube, FITS file. Then instruct the python compiler to execute the packing using a minimum value [min_value], a minimum delta [min_delta], and the minimum number of pixels [min_npix], while showing the progress of the command[verbose] (Figure 10).

[min_value]: is the minimum value we choose based on the noise level in our data cube. If no value is set here, the dendrogram will automatically take into consideration all the pixels including noise, therefore resulting in false mapping of the data.

[min_delta]: is the value chosen to avoid including a local maxima that can only be generated due to noisy data.

[min_npix]: is an optional command that specifies the minimum number of pixels a structure should have to remain independent. Refer to Appendix 1 for the full code used.

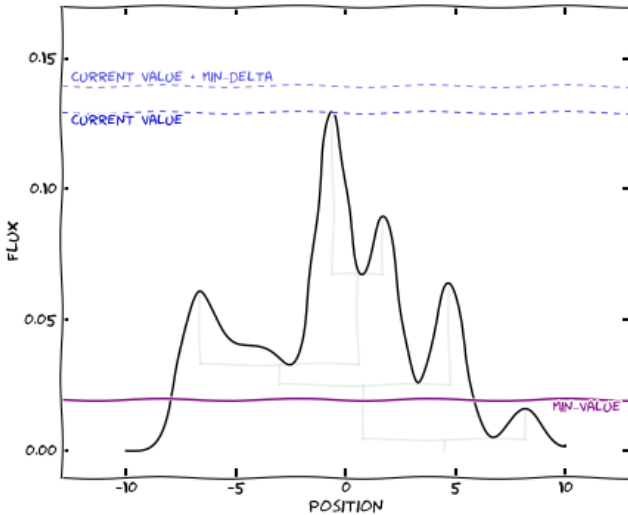


Figure 10: Showing a graph with a minimum mapping value towards the bottom and a delta band on top for scanning branches (Credits: Astrodendro)

2.5.2 Exploring a Dendrogram

Once the computation is complete, we can explore our data, identifying how many branches and leaves we have in a list view using [d] variable. The following is a code with an example output.

```
01 >>> d.trunk
[<Structure type=leaf idx=101>,
 <Structure type=branch idx=2152>,
 <Structure type=leaf idx=733>,
 <Structure type=branch idx=303>]
```

2.5.3 Saving and Loading a Dendrogram

There are two basic commands for saving or loading a dendrogram and there are:

```
>>> d.save_to('N42_dendrogram.fits')
```

```
>>> d = Dendrogram.load_from('N42_dendrogram.fits')
```

2.5.4 Data Output and Visualization

The Astrodendro package allows for data visualization and the ability to export these layers to other software such as DS9 for further analysis. The command used to visualize the mapped data cube is as follows:

```
d = Dendrogram.compute(...)  
v = d.viewer()  
v.show()
```

Once all the steps have been successfully completed a full analysis can be accomplished to conclude and achieve the aims of the research.

2.6 Moment Maps

A data cube is a file that contains observed data in x , y , and v axis. Where x and y represent the two sky coordinates axis, while v is the velocity line channel. You can think of a data cube as a stack of 2-dimensional images observed at different velocities. Moments are a good way to reduce the data cube into a map that can be easily studied. Every single pixel in the data cube gets processed to generate the required moment map resulting in maps with physical significance. This is best done by collapsing the data cube into a single image by taking a linear combination of each individual plane. For

a Pixel (i) and a velocity channel (k) where (w) is the spectral unit, and (I) is the cube:

$$M_m(x_i, y_i) = \sum_k^N w_m(x_i, y_i, v_k) I(x_i, y_i, v_k)$$

0th moment map, the integrated value of the spectrum - indicates the gas concentration at each pixel. This is a good way to examine a molecular cloud as it visually shows the clouds structure in terms of clumpy and filamentary areas.

$$M_0 = \Delta v \sum I_i$$

1st moment map, the intensity weighted coordinate - indicates if the molecular cloud is moving towards or away from the observer (red or blue shifted).

$$M_1 = \frac{\sum I_i v_i}{M_0}$$

CASA, will be used for generating moment maps. Refer to Appendix 1 to view the code used.

2.7 Clumps Mass

There are three cases that deal with cloud masses. If the mass of the cloud is estimated to be equal to its virial mass, then it should be close to virial equilibrium. On the other hand, if the mass is lower, then its assumed

that the cloud will disperse as its not gravitationally bound. If the clouds mass is greater, then the cloud will collapse unless supported by external factors.

Assuming that the cloud is gravitationally bound, the virial theorem applies, and the clumps to be spherical; clumps masses are calculated using the following equation (where σ is the velocity dispersion, and R is radius):

$$M_{Vir} \sim \frac{\sigma^2 R}{G}$$

The above equation can be simplified and used as follows (Wong et al. 2011):

$$M_{Vir} \sim 1040 \sigma^2 R_{pc}$$

2.8 Velocity Dispersion-Size Relationship

Some observational studies of molecular clouds suggest a scaling relationship between the mass, radii and velocity dispersion of the cloud. (Larson, 1981). These empirical relations apply both to the clouds as a whole and to substructures within the cloud. The statistical results found by Larson shows a correlation between velocity dispersion and the radius as follows:

$$\left(\frac{\delta v}{km s^{-1}} \right) = 1.1 \left(\frac{L}{pc} \right)^{0.38}$$

Following Larson's approach, many studies focusing on the velocity dispersion-size relationship have followed. These studies revealed that a power law index of 0.25 to 0.75 is observed for self-gravitating molecular

clouds in virial equilibrium. This will be used to compare the results of N42 against Larson’s power fit and compared with other molecular clouds in the region (Figure 11) (Dame et al., 1986; Heyer et al., 2001 & 2009; Hobson, 1992; Ikeda et al., 2009; Myers, 1983; Neelamkodan et al., 2018; Solomon et al., 1987; Tatematsu et al., 1998; Zhou et al.,1989).

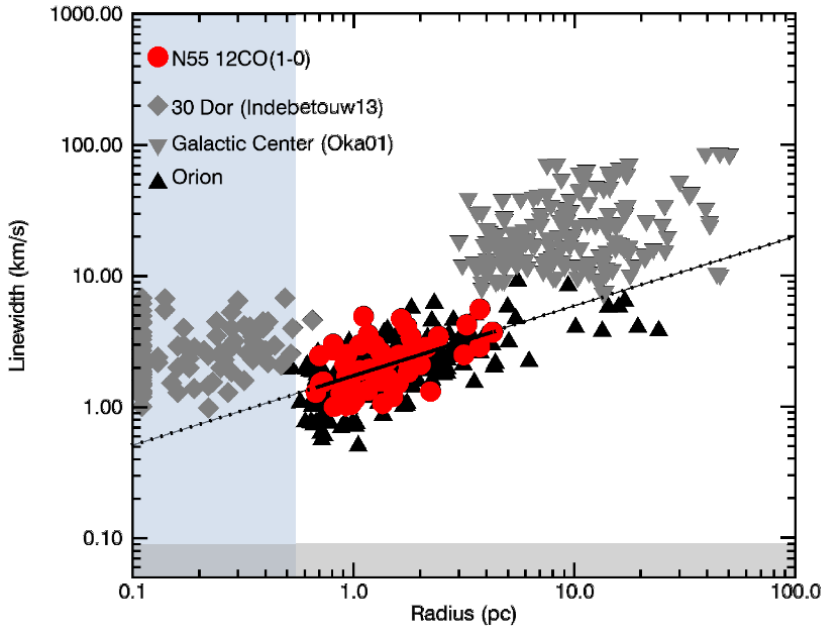


Figure 11: N55 clumps following a power law relation of 0.5 (Credits: Neelamkodan et al. 2018)

Chapter 3: Results

3.1 Integrated Value of the Spectrum

Looking at the integrated value of the spectrum map (0th moment map) we can immediately determine the areas with the highest gas concentrations (Figure 12), these massive clumps are the first indicator of an active star forming region. Over all, the area is clumpy and filamentary. This observation is similar what can be found in other metal-poor molecular clouds in the LMC and many clouds in Milky Way such as Orion and N55.

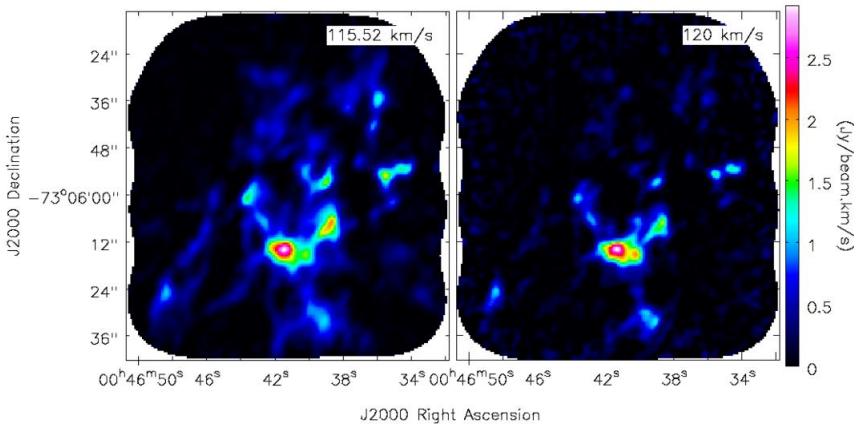


Figure 12: CASA output of N42 $^{12}\text{CO}(2-1)$ Moment 0 map left, and $^{13}\text{CO}(2-1)$ Moment 0 map right

3.2 Clumps Mass and Location

Using Astrodendro, a full list of clumps, velocities and locations are generated in a hierarchy of trunks and leaves. Refer to Appendix 2 for the full data output. To validate the results, we plot them over the 0th moment map. (Figure 13). It is clear that astrodendro's results are accurate and visually match the 0th moment map in identifying clumpy areas.

Knowing the exact location of clump is helpful in determining the any YSO association with specific clumps in the area. Browsing through VizieR Catalogues, a service that hosts astronomical catalogues, YSO's in the area are pinpointed and compared to the clumps the N42 molecular cloud (Figure 14).

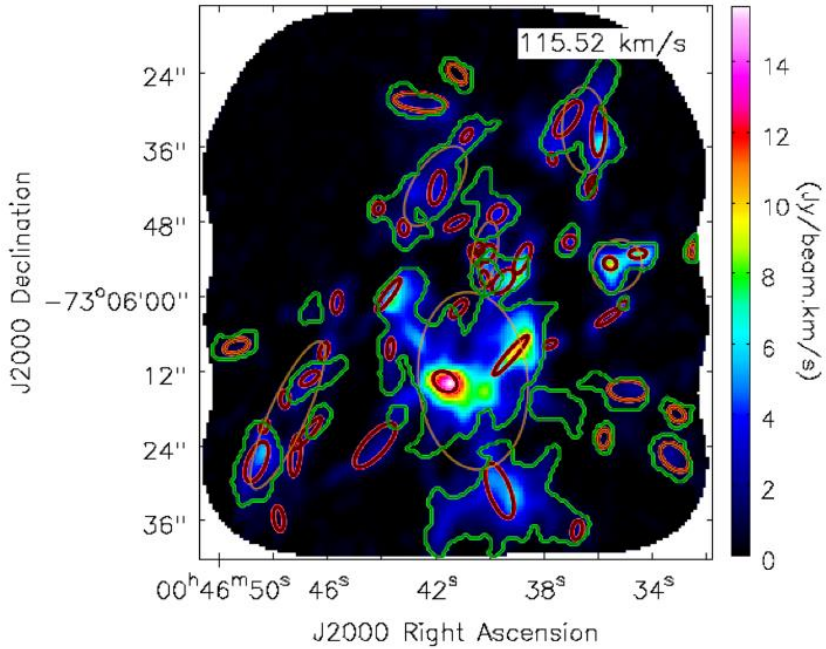


Figure 13: Detected clumps in the area. Green: N42 contours. Orange: AstroDendro computed trunks. Red: AstroDendro computed leaves.

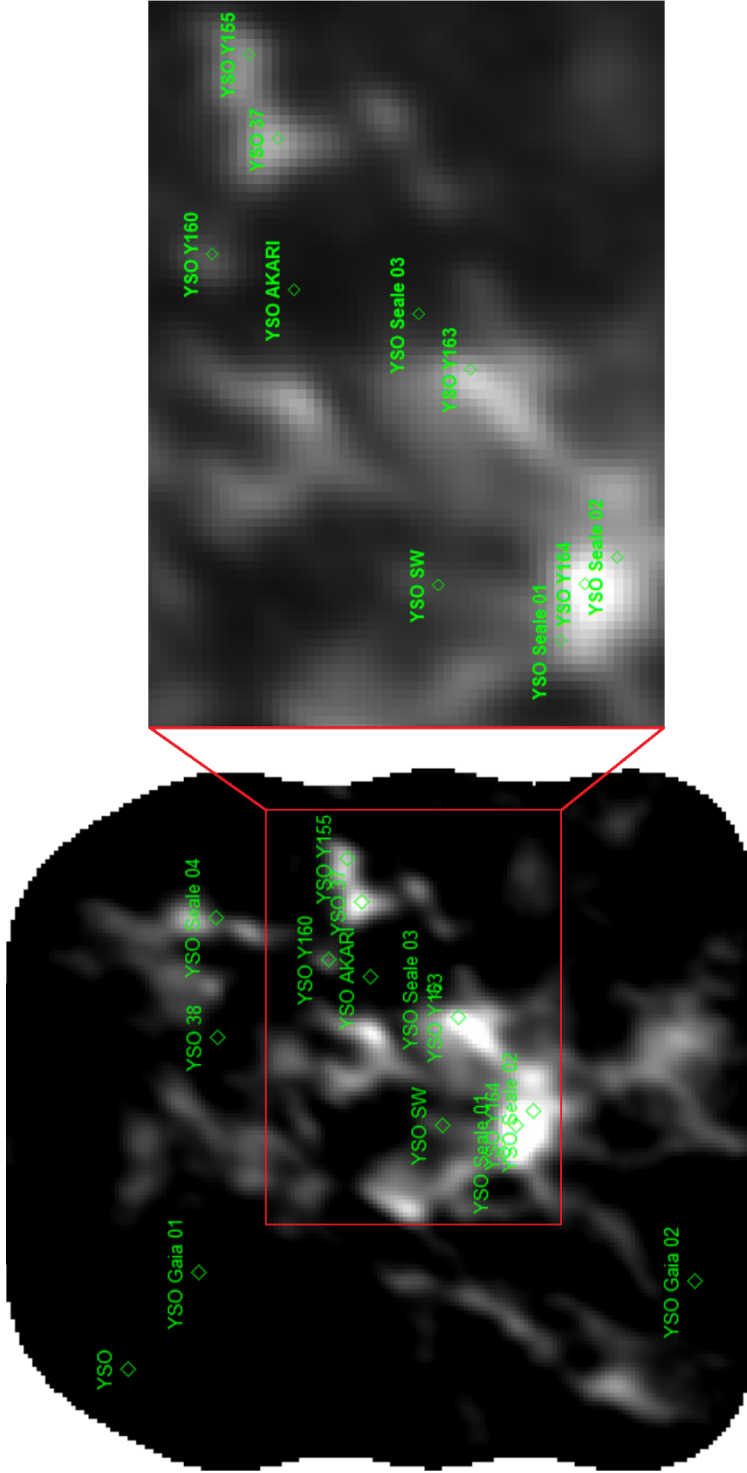


Figure 14: Plot of YSO's found in the region

Listing the YSO's in the region and comparing it with the exact position of the detected clump we can determine if the location of the YSO's is associated with the detected dense clumps in the region and check for any shift in position between the two as shown in Table 1.

Table 1: List of YSO's and clumps association.

No.	Name	Catalog	Clump association	Clump mass M_{\odot}	Offset in arcsec
1	Y164	<u>Sewilo+, 2013</u>	Yes	236	0.72
2	Y163	<u>Sewilo+, 2013</u>	Yes	184	1.15
3	Y160	<u>Sewilo+, 2013</u>	Yes	268	0.72
4	Y155	<u>Sewilo+, 2013</u>	Yes	153	0.54
5	Toth 01	<u>Toth+, 2014</u>			
6	Seale 01	<u>Seale+, 2014</u>			
7	Seale 02	<u>Seale+, 2014</u>			
8	Seale 03	<u>Seale+, 2014</u>			
9	Seale 04	<u>Seale+, 2014</u>	Yes	362	3.24
10	38	<u>Bolatto+, 2007</u>			
11	37	<u>Bolatto+, 2007</u>	Yes	154	0.72
12	SW	<u>Takekoshi+, 2017</u>			
13	Gaia 01	<u>Marton+, 2019</u>			
14	Gaia 02	<u>Marton+, 2019</u>			

3.3 Velocity Dispersion-Size Relationship

The velocity dispersion-size relationship for N42 is compared to other data obtained from other molecular clouds, including the galactic center (Figure 15). The red dashed line is based on Larson's scaling while the solid black line represents the N42 best fit line. When compared to Larson's, N42 results in the following:

$$\left(\frac{\delta v}{\text{km s}^{-1}}\right) = a \left(\frac{L}{\text{pc}}\right)^b$$

$$a = 0.546 \pm 0.036, \quad b = 0.409 \pm 0.120$$

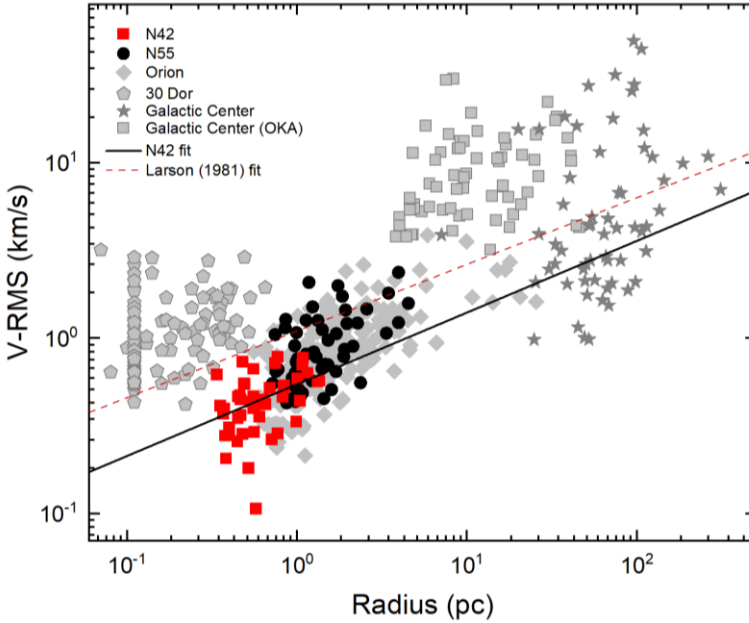


Figure 15: Velocity Dispersion-Size Relationship for $^{12}\text{CO}(2-1)$ in N42 compared to the galactic center, N55, Orion, and 30 Doradus clouds

N42 shows a similar trend as N55 in the LMC and Orion cloud in the Milky Way. This trend indicates a gravitational equilibrium of the clouds in N42 suggesting that clouds are virialized. Certain other clouds such as the Galactic center and 30 Doradus show a deviation from the general trend shown for virial equilibrium. This can be due to high turbulence in Galactic center and 30 Doradus due to immense star formation or due to some external pressure caused by a magnetic field (Field et al., 2011; Indebetouw et al., 2013; Oka et al., 2001).

3.4 Comparison of ^{12}CO Emission with H- α and Spitzer IRAC 8.0 μm

H- α map, a map that depicts the brightest hydrogen line in the visible spectral range is used to trace the ionized hydrogen content of molecular gas clouds. When N42 contours are overlaid on an H- α map (Figure 16) we observe that the cloud on the surface and away from the H- α emissions. This supports the classical picture of HII region and molecular cloud distributions, where we find a transition from the ionized gas surrounding the O stars to the molecular cloud. We expect the photo-dissociation region to be at the interface between the HII region and molecular cloud. To trace the photo-dissociation region we compare the distribution of polycyclic aromatic hydrocarbon emission (PAH) traced by Spitzer 8:0micron emission.

When looking at Spitzer's IRAC 8.0 μm map (Figure 17), a map that shows PAH emission, we observe that it is almost identical to the $^{12}\text{CO}(2-1)$ emission of N42. PAH, is widely observed in star forming regions as it influences the thermal budget of the interstellar medium by controlling the ionization balance (Li, 2020) However, in order to spatially resolve the transition from HII to PDR, we need a higher spatial resolution observation of HII region and PDR tracers.

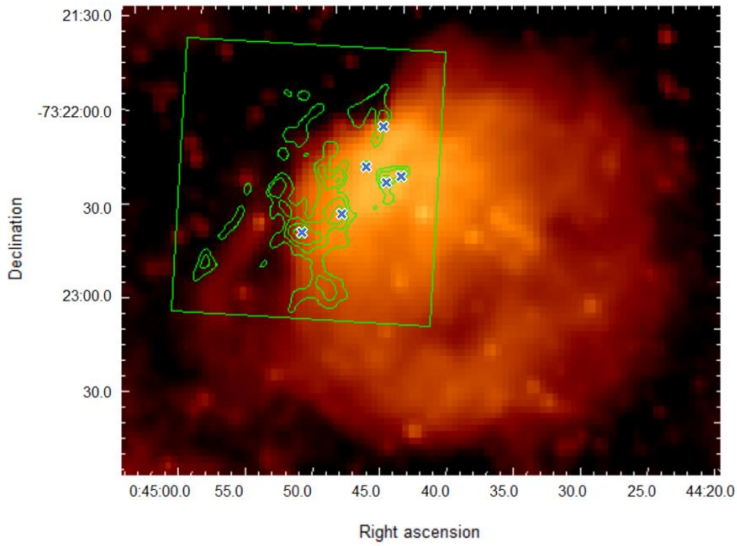


Figure 16: H- α map of N42 along with $^{12}\text{CO}(2-1)$ emission in contour of N42 with YSOs location represented as a blue cross

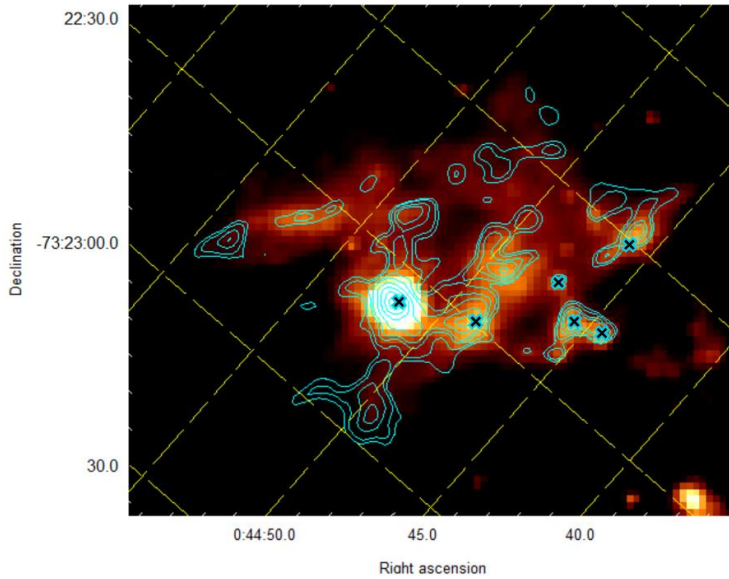


Figure 17: Spitzer 8.0 μm map of N42 along with $^{12}\text{CO}(2-1)$ emission in contour of N42 with YSOs location represented as a blue cross

3.5 Intensity Weighted Coordinate Map

Moment 1 maps are 1st moment intensity weighted velocity maps. This is useful to study the velocity structures in the cloud. The 1st moment map of N42 shows, the clouds in N42 over a velocity range 120 – 130 km/s (Figure 18). We find multiple velocity components in ¹²CO and ¹³CO molecular line profiles associated with a few clumps. These can be the indication of cloud-cloud collision that forms new massive stars as reported in Neelamkodan et al. (2021) and Fukui et al. (2015, 2016). The collision is suspected to be between a diagonal blue shifted area colliding with a vertical red shifted area. At the center of the collision, we have the densest cores measured previously by astrodendro. Multiple velocity components in line profiles can also be an indication of molecular outflow associated with protostars. The outflow is visible as a vertical extension from the center of the cloud towards the bottom center ending with a bulge. The outflow is similar to is reported by other cloud-cloud collisions reported in N66N, N159E, N159W south, and NGC 604 (Neelamkodan et al., 2018; Fukui et al., 2018; Muraoka et al., 2020; Tokuda et al., 2019).

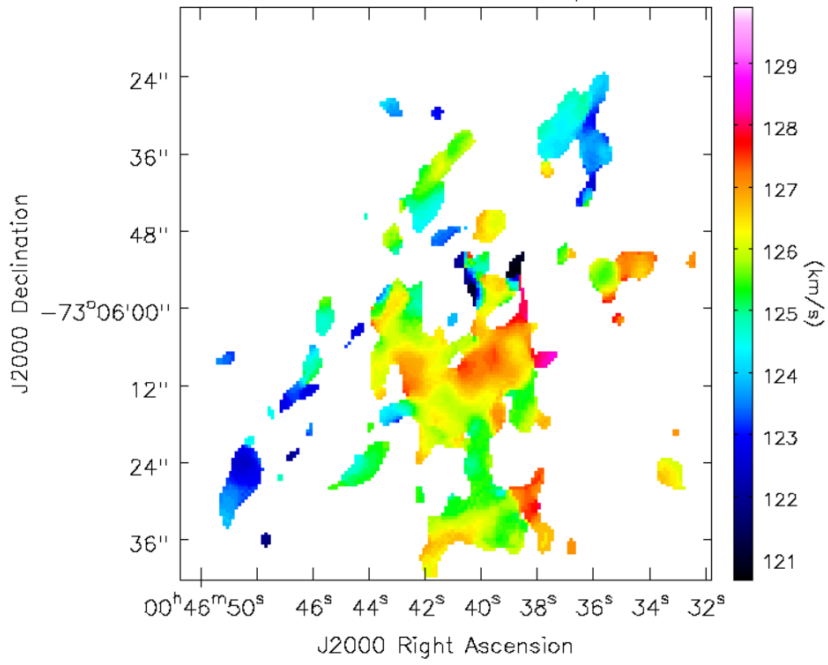


Figure 18: 1st Moment map of N42 $^{12}\text{CO}(2-1)$ emissions

Chapter 4: Discussion

4.1 Virial Mass Distribution

The clump with the largest virial mass associated with a YSO is measured to be $361.75 M_{\odot}$. There are a total of seven larger clumps averaging $500.21 M_{\odot}$ with the largest clump having a virial mass of $671.12 M_{\odot}$. These clumps may develop into a YSO in the future by self-gravitation. The overall average clump virial mass is $171.41 M_{\odot}$, while the average for YSO associated clumps is $226.20 M_{\odot}$.

4.2 Histograms of ^{12}CO Emissions

When looking at the ^{12}CO emission of N42 (Figure 19) you find that the mass of the clumps associated with YSOs falls in the region between $100 M_{\odot}$ and $400 M_{\odot}$ and the clumps with YSOs show large velocity dispersions. This result is similar to the trend found in the N55 cloud in the Large Magellanic Cloud. This can be due to the effect of certain turbulence in the cloud caused by YSO activity. However there seems to be no trend for associating YSOs and the cores radius.

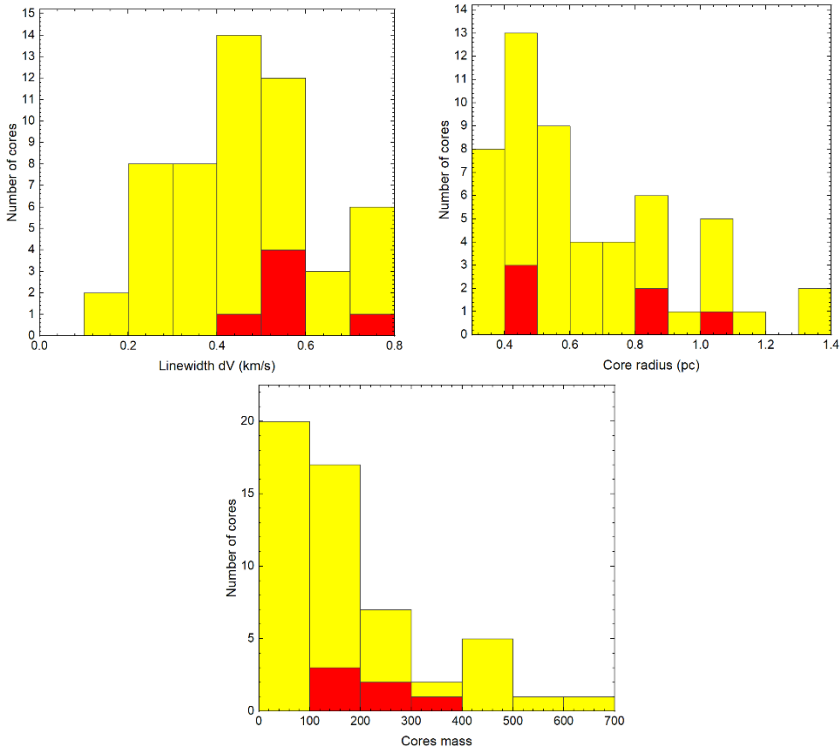


Figure 19: Cores with YSOs (red) and without (yellow). Left core linewidths. Right Core radius. Below: Cores mass

4.3 Clump/YSO Offset

The clumps associated with YSO's have an average south-easterly offset of an average of 0.77 arcsec, excluding the YSO from the Seale catalog, as it has an extreme offset of 3.25 arcsec. These offsets might initially represent the natural offset observed in the development of YSO's but I believe it to be the results of catalog data misalignment. This can be clearly observed from the reference given in the Seale catalog as it falls in an area with a low gas concentration.

4.4 Velocity Dispersion-Size Relationship

The results obtained for the power law index is 0.409 with an error of ± 0.120 which confirms with Myers range of 0.25 – 0.75 and is slightly higher than that estimated by Larson at 0.38. Regardless, the power fit line of N42 is a result of a clumps radius multiplied by half of that of Larsons, resulting in a lower fits line. This may be due to the state of molecular cloud. To confirm if N42 is virilized completely or not it would be required to cross check ^{12}CO and ^{13}CO clump masses with that of IMF to confirm virilization stage of the cloud.

4.5 H- α Map

The overlay of ^{12}CO contour emissions of N42 molecular cloud over the H – α emission map show that the cloud is on the surface. The gap between the molecular cloud and the HII region is known as the photo-dissociation region (Figure 20).

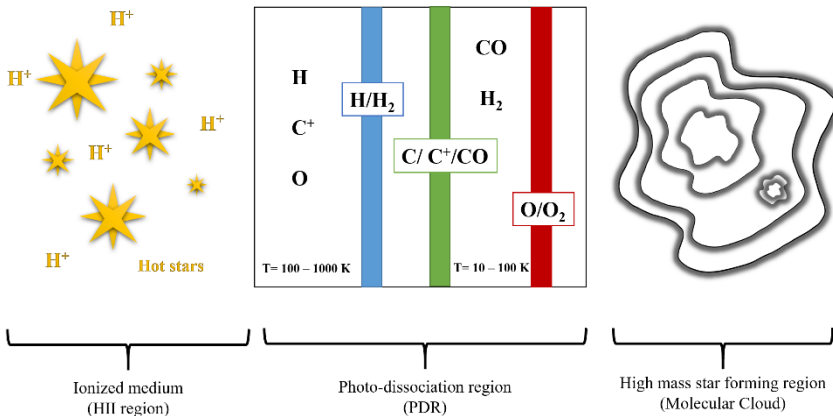


Figure 20: Photo-dissociation region

Chapter 5: Conclusion

5.1 Molecular Cloud Properties

The N42 molecular cloud is a clumpy star forming region. The dendrogram analysis on $^{12}\text{CO}(2-1)$ and $^{13}\text{CO}(2-1)$ emissions provide cloud properties such as size, velocity dispersion, and mass of N42. The clumps in this region have a . The average clump virial mass is $171.41 M_{\odot}$, while it is $226.20 M_{\odot}$ for YSO associated clumps. The clumps radius ranges between 0.34 to 1.35 pc with an average of 0.65 pc. It is found that the molecular cores (generated by dendrogram leaves) that are associated with YSOs exhibit a larger mass and velocity. It is found that 30% of massive cores $> 150 M_{\odot}$ are associated with YSOs.

5.2 Distribution of Molecular Gas

The molecular gas distribution is clumpy and filamentary as observed in the $^{12}\text{CO}(2-1)$ and $^{13}\text{CO}(2-1)$ of the integrated value of the spectrum map. The same distribution is also seen and validated using Spitzer's $8.0 \mu\text{m}$ polycyclic aromatic hydrocarbon (PAH) emission map.

5.3 Velocity Dispersion-Size Relationship

The Velocity dispersion-size relationship resulted in a power law with an index of 0.41 ± 0.1 . This is consistent with the results obtained from N55 cloud and Orion cloud measured at similar spatial scales. The supports the argument that N42 is gravitationally bound without the interference of external pressures.

5.4 Intensity Weighted Coordinate Map

The Intensity weighted Coordinate Map indicates a cloud-cloud collision based on the blue/red shifted but would require further studied to

confirm this assumption. The cores associated with YSOs show a multipeak profile indicating YSO activities.

References

- Beuther, H., Churchwell, E. B., McKee, C. F., et al. (2007) The Formation of Massive Stars. *Protostars and Planets V*, 165.
- Bonnell, I. A., Bate, M. R., & Zinnecker, H. (1998). On the Formation of Massive Stars. *Monthly Notices of the Royal Astronomical Society*, 298(1), 93-102.
- Bonnell, I. A., Bate, M. R., Clarke, C. J., et al. (1997). Accretion and the Stellar Mass Spectrum in Small Clusters. *Monthly Notices of the Royal Astronomical Society*, 285, 201-208.
- Bonnell, I. A., Vine, S. G., & Bate, M. R. (2004). Dynamical Models of Star Formation and the Initial Mass Function. *Monthly Notices of the Royal Astronomical Society*, 349, 735-741.
- Clarke, C. J., Bonnell, I. A., & Hillenbrand, L. A. (2000). The Formation of Stellar Clusters. *Proto-stars and Planets IV*, 151.
- Dame, T. M., Elmegreen, B. G., Cohen, R. S., & Thaddeus, P. (1986). The Milky Way in Molecular Clouds: A New Complete CO Survey. *The Astrophysical Journal*, 547, 792-813.
- Edgar, R., & Clarke, C. (2003). Feedback in Star Formation Simulations: Implications for the IMF. *Monthly Notices of the Royal Astronomical Society*, 338, 962-972.
- Field et al. (2011). Does External Pressure Explain Recent Results for Molecular Clouds? *Monthly Notices of the Royal Astronomical Society*, 416, 710-714.
- Fukui, Y., Harada, R., Tokuda, K., et al. (2015). High-Mass Star Formation Triggered by Collision Between Co Filaments in N159 West in The Large Magellanic Cloud. *The Astrophysical Journal Letters*, 807, L4.
- Fukui, Y. et al. (2016). The Two Molecular Clouds in RCW 38: Evidence for the Formation of the Youngest Super Star Cluster in the Milky

- Way Triggered by Cloud–Cloud Collision. *The Astrophysical Journal*, 26:DOI:10.3847/0004-637X/820/1/26.
- Fukui, Y. et al. (2018). The Formation of Massive Molecular Filaments and Massive Stars Triggered by a Magnetohydrodynamic Shock Wave. *Astronomical Society of Japan*, 70, SP2, S53:DOI:10.1093/pasj/psx089.
- Heyer, M. H., Carpenter, J. M., & Snell, R. L. (2001). The Equilibrium State of Molecular Regions in the Outer Galaxy. *The Astrophysical Journal*, 551, 852-866.
- Hills, R. R., & Beasley, A. J. (2008). “The Atacama Large Millimeter/submillimeter Array,” in Ground-based and Airborne Telescopes II. *National Radio Astronomy Observatory SPIE*, 7012, 7012N.
- Hobson, M. P. (1992) High-resolution HCO⁺ and HCN Observations of M17SW: Clumps, Turbulence and Cloud Support. *Monthly Notices of the Royal Astronomical Society*, 256, 457-476.
- Hollenbach, D. J., & Tielens, A. G. G. M. (1997). Dense Photodissociation Regions (PDRs). *Annual Review of Astronomy and Astrophysics*, 35, 179-215.
- Ikeda, N., Kitamura, Y., & Sunada, K. (2009). Similarity Between the C18o (J = 1-0) Core Mass Function and the Initial Mass Function (IMF) in the S140 Region. *The Astrophysical Journal*, 691, 101:DOI:10.1088/0004-637X/732/2/101.
- Indebetouw, R., Brogan, C., Chen, C.-H. R., et al. (2013). Alma Resolves 30 Doradus: Sub-Parsec Molecular Cloud Structure Near the Closest Super Star Cluster. *The Astrophysical Journal*, 774, 73:DOI:10.1088/0004-637X/774/1/73.
- Inoue, T., & Fukui, Y. (2013). Formation of Massive Molecular Cloud Cores by Cloud-Cloud Collision. *The Astrophysical Journal Letters*, 774, L31:DOI:10.1088/2041-8205/774/2/L31.
- Johnstone et al. (2006). Cold Molecular Gas in the Perseus Cluster Core. *Astronomy & Astrophysics*, 454, 437-445.

- Kawamura, A., Onishi, T., Yonekura, Y., et al. (1998). A 13CO Survey of Molecular Clouds in Gemini and Auriga. *Astronomical Society of Japan*, 117, 313-339.
- Krumholz, M. R. (2014). The Big Problems in Star Formation: the Star Formation Rate, Stellar Clustering, and the Initial Mass Function. *Physics Reports*, 539, 49-134.
- Larson R. B. (1981). Turbulence and Star Formation in Molecular Clouds. *Monthly Notices of the Royal Astronomical Society*, 194(4), 809-826.
- Li, A. (2020) Spitzer's Perspective of Polycyclic Aromatic Hydrocarbons in Galaxies. *Nature Astronomy* 4, 339-351.
- Lundgren, A. et al. (2012). "ALMA: the First Year of Observations," in Observatory Operations: Strategies, Processes, and System IV, *National Radio Astronomy Observatory SPIE*, 8448, 844802.
- Motte, F., Andre, P., & Neri, R. (1998). The Initial Conditions of Star Formation in the Rho Ophiuchi Main Cloud: Wide-Field Millimeter Continuum Mapping. *Astronomy & Astrophysics*, 336, 150-172.
- Motte, F., Bontemps, S., & Louvet, F. (2018) High-Mass Star and Massive Cluster Formation in the Milky Way. *Annual Review of Astronomy and Astrophysics*, 56, 41-82.
- Muraoka, K., Kondo, H., Tokuda, K., et al. (2020). ALMA Observations of Giant Molecular Clouds in M33. II. Triggered High-mass Star Formation by Multiple Gas Colliding Events at the NGC 604 Complex, *The Astrophysical Journal*, 903, 94:DOI:10.3847/1538-4357/abb822.
- Myers, P. C. (2009). Filamentary Structure of Star-forming Complexes. *The Astrophysical Journal*, 700, 1609:DOI:10.1088/0004-637X/700/2/1609.
- Neelamkodan, Tokuda, K., Onishi, T., et al. (2018). ALMA Reveals Molecular Cloud N55 in the Large Magellanic Cloud as a Site of

- Massive Star Formation. *The Astrophysical Journal*, 853, 175:DOI:10.3847/1538-4357/aaa5b0.
- Nayana, J, Neelamkodan , Onishi T., et al. (2020). ALMA Observations of HCO+ and HCN Emission in the Massive Star-forming Region N55 of the Large Magellanic Cloud. *The Astrophysical Journal*, 902, 140:DOI:10.3847/1538-4357/abb466.
- Oka, T., Hasegawa, T., Sato, F., et al. (2001). Statistical Properties of Molecular Clouds in the Galactic Center. *The Astrophysical Journal*, 562, 348:DOI:10.1086/322976.
- Onishi, T., Mizuno, A., Kawamura, A., et al. (2002). A Complete Search for Dense Cloud Cores in Taurus. *The Astrophysical Journal*, 575, 950:DOI:10.1086/341347.
- Scoville et al. (1986). High-Mass Star Formation Due to Cloud-Cloud Collisions. *The Astrophysical Journal* ,310, L77:DOI:10.1086/184785.
- Solomon, P. M., Rivolo, A. R., Barrett, J., & Yahil, A. (1987). Mass, Luminosity, and Line Width Relations of Galactic Molecular Clouds. *The Astrophysical Journal*, 319, 730:DOI:10.1086/165493.
- Solomon, P. M., et al. (1989). A Face-On View of the First Galactic Quadrant in Molecular Clouds. *The Astrophysical Journal*,339, 919:DOI:10.1086/167345.
- Spitzer, L. (1978) *American Scientist*, 66, 426.
- Tatematsu et al. (1998). Molecular Cloud Cores in the Orion A Cloud. II. FCRAO CS (2-1) Data. *The Astrophysical Journal Supplement Series*, 118(2), 517-539.
- Tokuda, K., Fukui, Y., Harada, R., et al. (2019). An ALMA View of Molecular Filaments in the Large Magellanic Cloud. II. An Early Stage of High-mass Star Formation Embedded at Colliding Clouds in N159W-South, *The Astrophysical Journal*, 886, 15:DOI: 10.3847/1538-4357.

- Westerlund B. E. (1991). Proc IAU Symp. 148, The Magellanic Clouds. Kluwer, Dordrecht.
- Wong, T., Hughes, A., Ott, J., et al. (2011). The Magellanic Mopra Assessment (MAGMA). I. The Molecular Cloud Population of the Large Magellanic Cloud. *Astrophysical Journal Supplement*, 197, 16:DOI:10.1088/0067-0049/197/2/16.
- Yonekura, Y., Dobashi, K., Mizuno, A., Ogawa, H., & Fukui, Y. A. (1997) 13CO Survey of Molecular Clouds in Gemini and Auriga. *Astronomical Society of Japan*, 56(2), 313-339.
- Yorke, H. W., & Sonnhalter, C. (2002) On the Formation of Massive Stars. *The Astrophysical Journal*, 569, 846:DOI:10.1086/339264.
- Zhou et al. (1989). A CS Survey of Low-Mass Cores and Comparison with NH₃ Observations. *The Astrophysical Journal*, 346, 168:DOI: 10.1086/167997.
- Zinnecker, H., & Yorke, H. W. (2007). Toward Understanding Massive Star Formation. *Annual Review of Astronomy and Astrophysics*, 45, 481-563.

Appendix 1: List of Codes used

1.1 CASA 0th and 1st Moment Maps

```
from astrodendro import Dendrogram
from astrodendro import ppv_catalog
from astrodendro.analysis import PPVStatistic
from astropy.io import fits
from astropy import wcs
from astrodendro.scatter import Scatter
import matplotlib.pyplot as plt
from astropy import units as u
from xlwt import Workbook
import aplpy
import numpy
metadata={}
metadata['data_unit']=u.Jy/u.beam
metadata['spatial_scale'] = 0.5*u.arcsec # 1 pixel =
0.5 arcsec
metadata['beam_major'] = 2.6838*u.arcsec
metadata['beam_minor'] = 1.8953*u.arcsec
metadata['velocity_scale'] = 0.32*u.km/u.s
metadata['wcs'] = wcs
```

1.2 Astrodendro – Generating Dendrograms

```
from astrodendro import Dendrogram
from astrodendro import ppv_catalog
from astrodendro.analysis import PPVStatistic
from astropy.io import fits
from astropy import wcs
from astrodendro.scatter import Scatter
import matplotlib.pyplot as plt
from astropy import units as u
from xlwt import Workbook
import aplpy
import numpy
metadata={}
metadata['data_unit']=u.Jy/u.beam
metadata['spatial_scale'] = 0.5*u.arcsec # 1 pixel =
0.5 arcsec
metadata['beam_major'] = 2.6838*u.arcsec
metadata['beam_minor'] = 1.8953*u.arcsec
metadata['velocity_scale'] = 0.32*u.km/u.s
metadata['wcs'] = wcs
```

```

data, header = fits.getdata('n42.fits', header=True)
wcs = wcs.WCS(header)
metadata['wcs'] = wcs
rms=0.19 #Jy/beam
d = Dendrogram.compute(data, min_value=2*rms,
min_delta=2*rms, min_npix=1 ,verbose=True)

cat=ppv_catalog(d,metadata)
cat.pprint(show_unit=True, max_lines=40)
cat.pprint(show_unit=True, max_lines=40)

trunk_idx_list = []
for i in range(len(d.trunk)):
    trunk_idx_list.append(d.trunk[i].idx)

ar = numpy.arange(len(cat))
ar1 = list(ar)
all = trunk_idx_list
for i in range(len(d.trunk)):
    ar1.remove(all[i])

cat1 = cat.copy()
cat1.remove_rows([ar1])
cat1.write('N42_trunk.dat',format='ascii')

leaves_idx_list = []
for i in range(len(d.leaves)):
    leaves_idx_list.append(d.leaves[i].idx)

ar = numpy.arange(len(cat))
ar1 = list(ar)
all = leaves_idx_list
for i in range(len(d.leaves)):
    ar1.remove(all[i])

cat1 = cat.copy()
cat1.remove_rows([ar1])
cat1.write('N42_leaves.dat',format='ascii')

v = d.viewer()
v.show()

```

1.3 Astrodendro – Plotting Dendrograms on 0th Moment Map

```
from astrodendro import Dendrogram
from astrodendro import ppv_catalog
from astrodendro.analysis import PPVStatistic
from astropy.io import fits
from astropy import wcs
from astrodendro.scatter import Scatter
import matplotlib.pyplot as plt
from astropy import units as u
from xlwt import Workbook
import numpy
import aplpy

metadata={}
metadata['data_unit']=u.Jy/u.beam
metadata['spatial_scale'] = 0.5*u.arcsec # 1 pixel =
0.5 arcsec
metadata['beam_major'] = 2.6838*u.arcsec
metadata['beam_minor'] = 1.8953*u.arcsec
metadata['velocity_scale'] = 0.32*u.km/u.s
metadata['wcs'] = wcs

data, header = fits.getdata('n42.fits', header=True)
wcs = wcs.WCS(header)
metadata['wcs'] = wcs
rms=0.19 #Jy/beam
d = Dendrogram.compute(data, min_value=2*rms,
min_delta=2*rms, min_npix=1 ,verbose=True)

p = d.plotter()
from astrodendro.analysis import PPVStatistic
import matplotlib.pyplot as plt
from matplotlib.patches import Ellipse
image = fits.getdata('n42moment0.fits')

fig = plt.figure()
ax = fig.add_subplot(1, 1, 1)
ax.imshow(image, origin='lower',
interpolation='nearest', cmap=plt.cm.Blues)

for leaf in d.leaves:
    p.plot_contour(ax, structure=leaf, lw=2,
colors='red')
    s = PPVStatistic(leaf)
    ellipse = s.to_mpl_ellipse(edgecolor='red',
linewidth=2, facecolor='none')
    ax.add_patch(ellipse)
```

```
for trunk in d.trunk:
    p.plot_contour(ax, structure=trunk, lw=1,
        colors='green')
    s = PPVStatistic(trunk)
    ellipse = s.to_mpl_ellipse(edgecolor='orange',
        linewidth=1, facecolor='none')
    ax.add_patch(ellipse)

plt.show()

for trunk in d.trunk:
    p.plot_contour(ax, structure=trunk, lw=1,
        colors='green')
    s = PPVStatistic(trunk)
    ellipse = s.to_mpl_ellipse(edgecolor='orange',
        linewidth=1, facecolor='none')
    ax.add_patch(ellipse)

plt.show()
```

Appendix 2: N42 Astrodendro Output Table with Computed Clumps Virial Mass.

N42 $^{12}\text{CO}(2-1)$ - Leaves Data						
ID	RA	Dec	Radius (pc)	V-RMS	Mass (virial)	YSO Association
1	11.66159	-73.0984	0.769175	0.783041	490.4866	
2	11.66731	-73.0993	0.447965	0.348778	56.67281	
3	11.69887	-73.1099	0.600505	0.3572	79.68432	
4	11.69452	-73.1061	0.742303	0.722171	402.6194	
5	11.70223	-73.1074	1.073191	0.704856	554.5116	
6	11.66879	-73.0983	0.517197	0.181605	17.73972	
7	11.67718	-73.0915	1.150328	0.634538	481.6928	
8	11.65108	-73.095	0.368069	0.371633	52.86779	
9	11.64993	-73.0928	1.003101	0.588864	361.7502	YSO 04
10	11.69411	-73.1037	0.55091	0.398819	91.13115	
11	11.68206	-73.1	0.689177	0.520397	194.1036	
12	11.67134	-73.1006	0.562903	0.405363	96.19552	
13	11.67168	-73.0968	0.587496	0.443229	120.0314	
14	11.70533	-73.1023	0.708318	0.265051	51.75109	
15	11.69792	-73.1046	0.476609	0.284682	40.17131	
16	11.69195	-73.1025	0.460021	0.471142	106.1978	
17	11.65465	-73.0922	0.987746	0.335448	115.5926	
18	11.66509	-73.1087	1.349703	0.571912	459.1247	
19	11.69631	-73.1071	0.767583	0.287262	65.87417	
20	11.68412	-73.1066	1.318532	0.567694	441.9286	
21	11.70107	-73.1058	0.381505	0.206375	16.89845	
22	11.68992	-73.1003	0.55367	0.467339	125.7616	
23	11.66705	-73.0982	0.634983	0.444857	130.6884	
24	11.68359	-73.0962	0.397104	0.280158	32.41474	
25	11.6746	-73.0953	0.836689	0.53859	252.4146	
26	11.64819	-73.0986	0.489758	0.549489	153.792	YSO37
27	11.65426	-73.0977	0.477625	0.734916	268.2846	YSO160
28	11.65095	-73.0953	0.466759	0.364147	64.36945	
29	11.6734	-73.1038	0.832997	0.522111	236.1581	YSO164
30	11.67972	-73.097	0.463971	0.447965	96.83078	
31	11.6701	-73.093	0.398164	0.309259	39.60402	
32	11.66453	-73.0994	0.822683	0.463587	183.8775	
33	11.63827	-73.1072	1.040005	0.439435	208.8609	
34	11.64545	-73.1042	1.081782	0.772346	671.1159	
35	11.68178	-73.1024	0.444666	0.257702	30.71162	
36	11.66541	-73.0964	0.648624	0.419815	118.8889	
37	11.65703	-73.094	0.353419	0.412489	62.53859	
38	11.66337	-73.1027	0.82406	0.463713	184.2852	YSO163
39	11.64395	-73.0982	0.485157	0.550489	152.9018	YSO155
40	11.64616	-73.1004	0.337226	0.62151	135.4722	

41	11.65321	-73.1104	0.533562	0.434201	104.6166
42	11.63559	-73.098	0.372969	0.396137	60.8691
43	11.638	-73.1053	0.572433	0.106642	6.77035
44	11.66827	-73.098	0.450525	0.465326	101.4536
45	11.65737	-73.1022	0.378452	0.278108	30.44183
46	11.64844	-73.101	0.551617	0.668749	256.5654
47	11.64912	-73.1063	0.559429	0.292389	49.73929

N42 $^{12}\text{CO}(2-1)$ - Trunks Data					
ID	RA	Dec	Radius (pc)	V-RMS	Mass (virial)
1	11.66914	-73.1038	5.342551	1.341275	9995.80
2	11.66736	-73.0982	1.578722	0.661458	718.36
3	11.69749	-73.1053	2.946262	1.173109	4216.79
4	11.6521	-73.0927	2.383925	1.118552	3101.97
5	11.67718	-73.0915	1.150328	0.634538	481.69
6	11.67491	-73.0952	2.419493	1.107199	3084.67
7	11.70533	-73.1023	0.708318	0.265051	51.75
8	11.64711	-73.0987	1.951037	1.35273	3712.96
9	11.63827	-73.1072	1.040005	0.439435	208.86
10	11.64545	-73.1042	1.081782	0.772346	671.12
11	11.63559	-73.098	0.372969	0.396137	60.87
12	11.638	-73.1053	0.572433	0.106642	6.77
13	11.64912	-73.1063	0.559429	0.292389	49.74

UAEU

جامعة الإمارات العربية المتحدة
United Arab Emirates University



UAE UNIVERSITY MASTER THESIS NO. 2022:6

The research looks into Molecular cloud properties in high-mass star forming regions using the latest astrophysical tools and data to get a better understanding into the formation process of high-mass stars.

www.uaeu.ac.ae

Mohammed Ahli received his Master of Science in Physics from the Department of Physics, College of Science, at the United Arab Emirates University, UAE.